Supporting Information

Synthesis and Solution Stability of Water-Soluble κ^2*N*,κ*O*-Bis(3,5-dimethylpyrazolyl)ethanol manganese(I) tricarbonyl bromide (CORM-ONN1)

Ralf Mede,[a] Juliane Traber,[a] Moritz Klein,[b,c] Helmar Görls,[a] Guido Gessner,[d] Patrick Hoffmann,[c,e] Michael Schmitt,[b,c] Jürgen Popp,[b,c,e] Stefan H. Heinemann,[d] Ute Neugebauer,[b,c,e] Matthias Westerhausen*,[a]

Content:

[Bis(3,5-dimethyl-1-pyrazolyl)methane]Mn(CO)$_3$Br

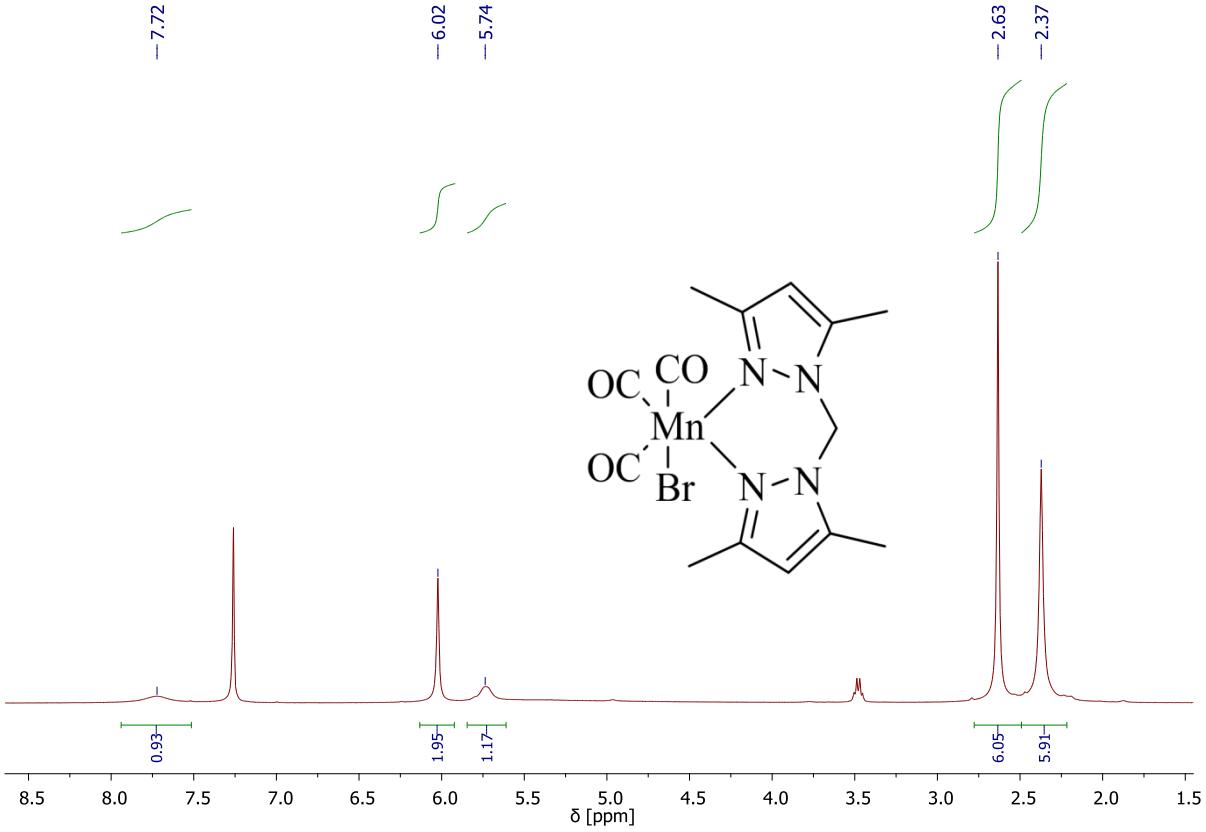

Figure S1: ^{1}H-NMR spectrum of [Bis(3,5-dimethyl-1-pyrazolyl)methane]Mn(CO)$_3$Br in $CDCl_3$.

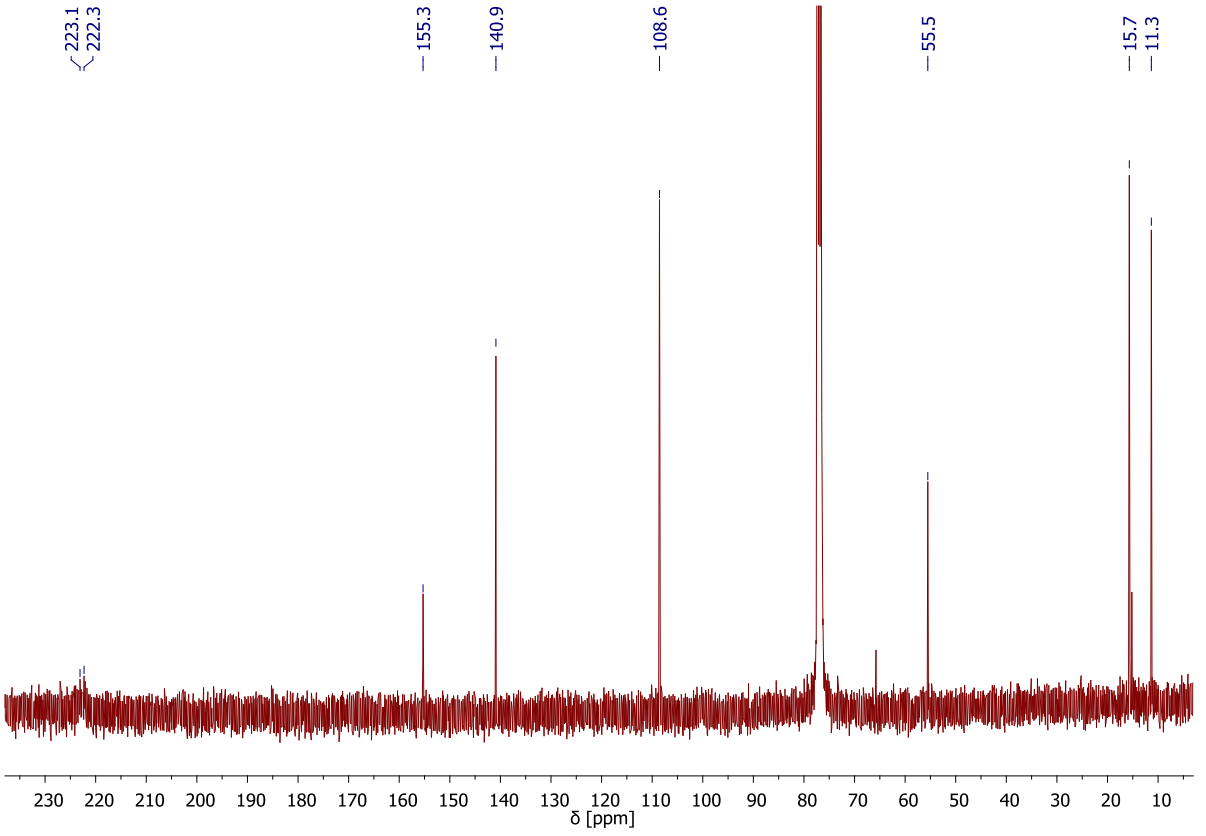

Figure S2: ^{13}C{^{1}H}-NMR spectrum of [Bis(3,5-dimethyl-1-pyrazolyl)methane]Mn(CO)$_3$Br in $CDCl_3$.

[Bis(3,5-dimethylpyrazol-1-yl)acetato]Mn(CO)$_3$

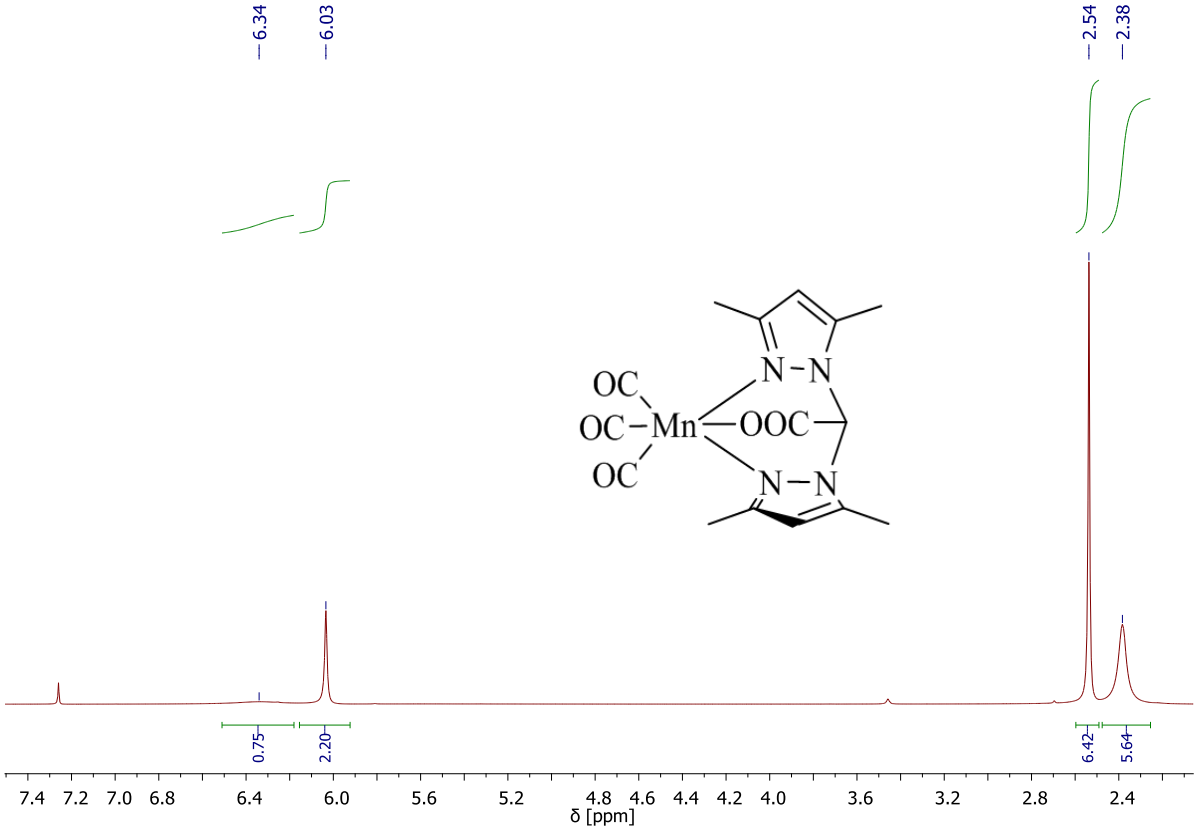

Figure S3: ^{1}H-NMR spectrum of [Bis(3,5-dimethylpyrazol-1-yl)acetate]Mn(CO)$_3$ in CDCl$_3$.

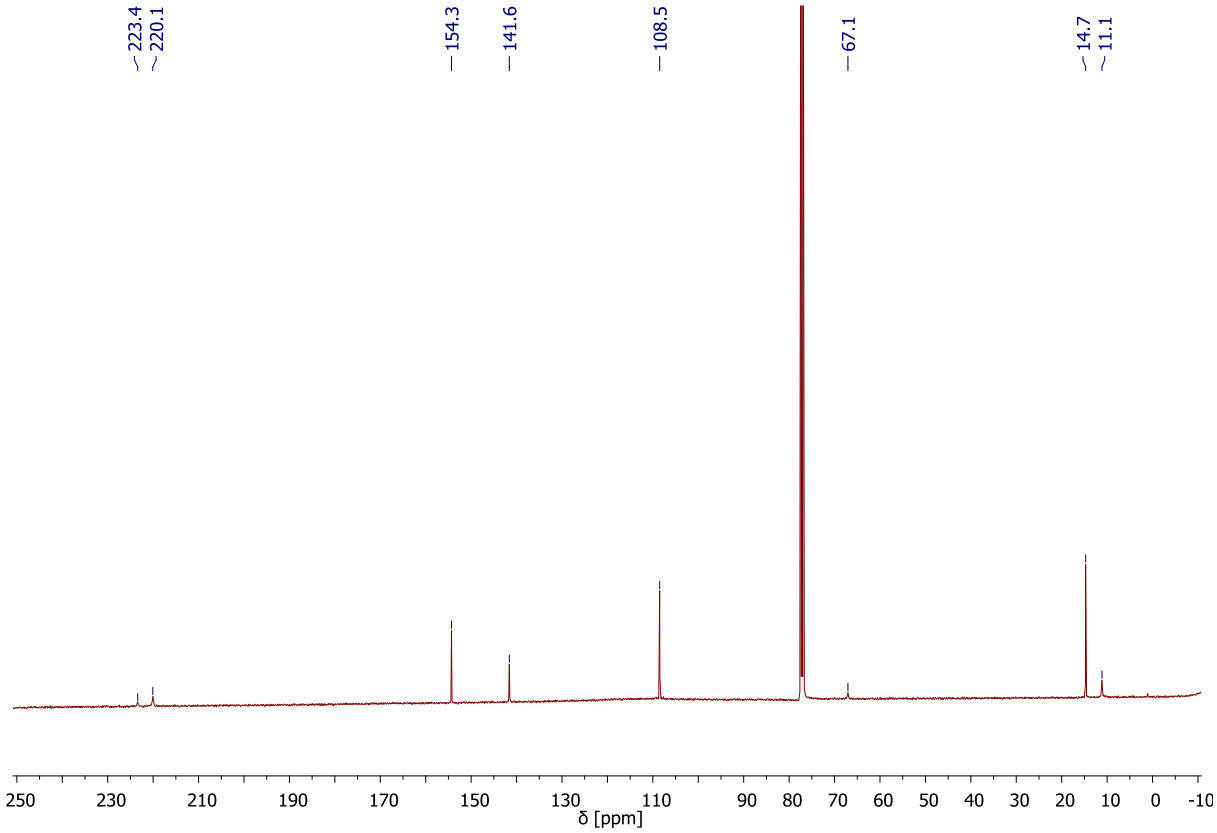

Figure S4: ^{13}C{^{1}H}-NMR spectrum of [Bis(3,5-dimethylpyrazol-1-yl)acetate]Mn(CO)$_3$ in CDCl$_3$.

2,2-Bis(3,5-dimethylpyrazol-1-yl)ethanol

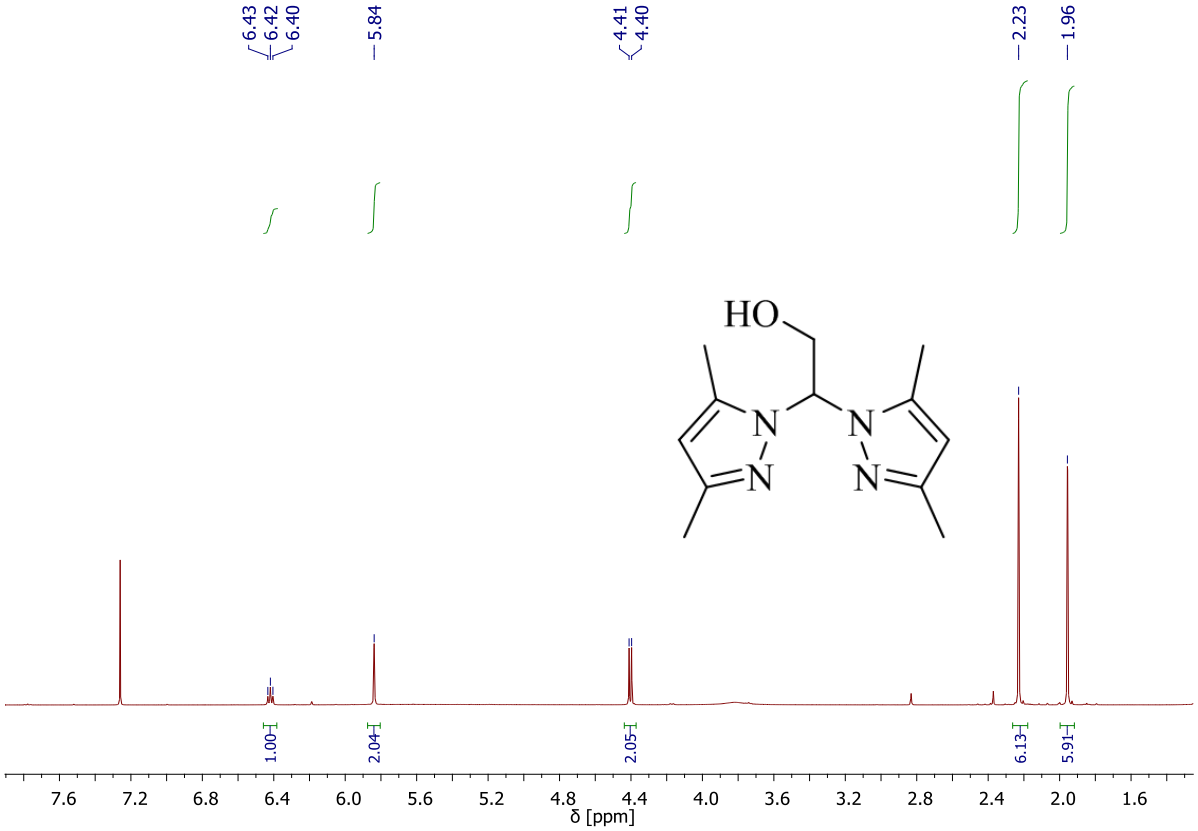

Figure S5: ^{1}H-NMR spectrum of 2,2-bis(3,5-dimethylpyrazol-1-yl)ethanol in $CDCl_3$.

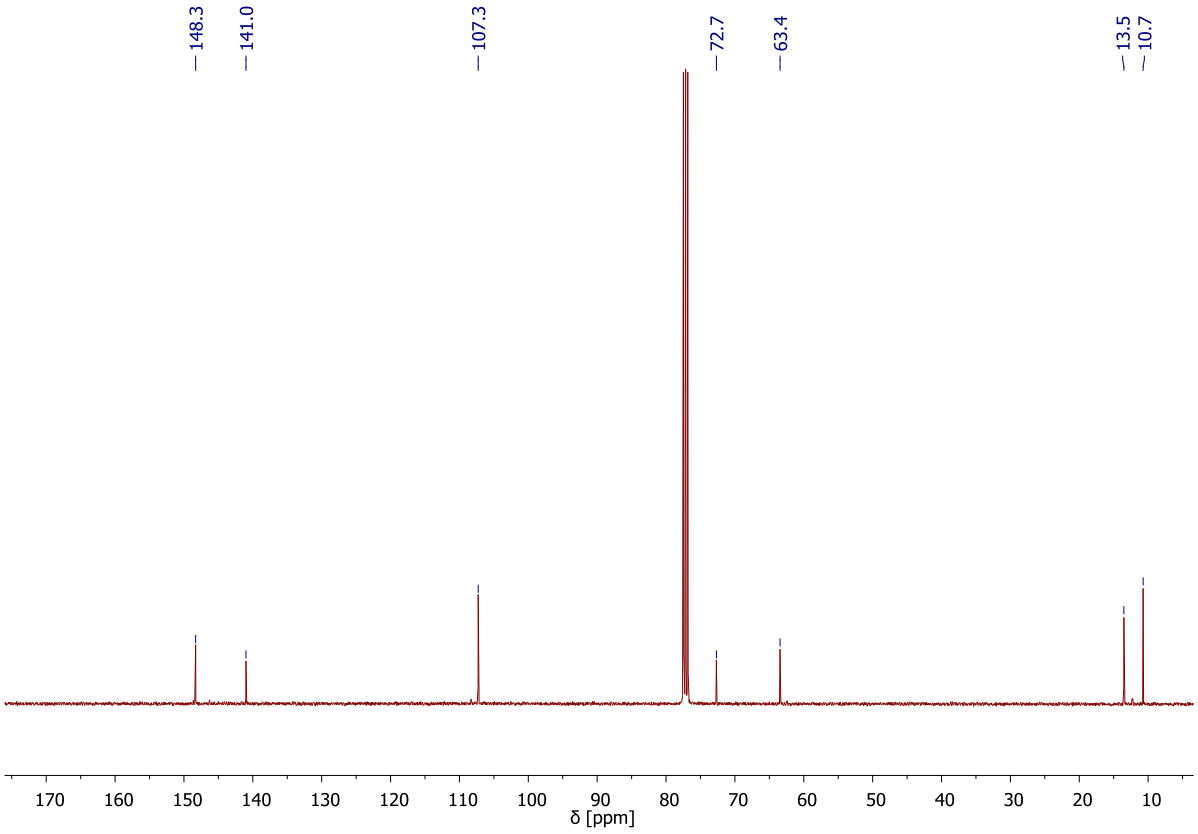

Figure S6: $^{13}C\{^{1}H\}$-NMR spectrum of 2,2-bis(3,5-dimethylpyrazol-1-yl)ethanol in $CDCl_3$.

[{2,2-Bis(3,5-dimethylpyrazol-1-yl)ethanol}Mn(CO)$_3$]Br (CORM-ONN1, 3)

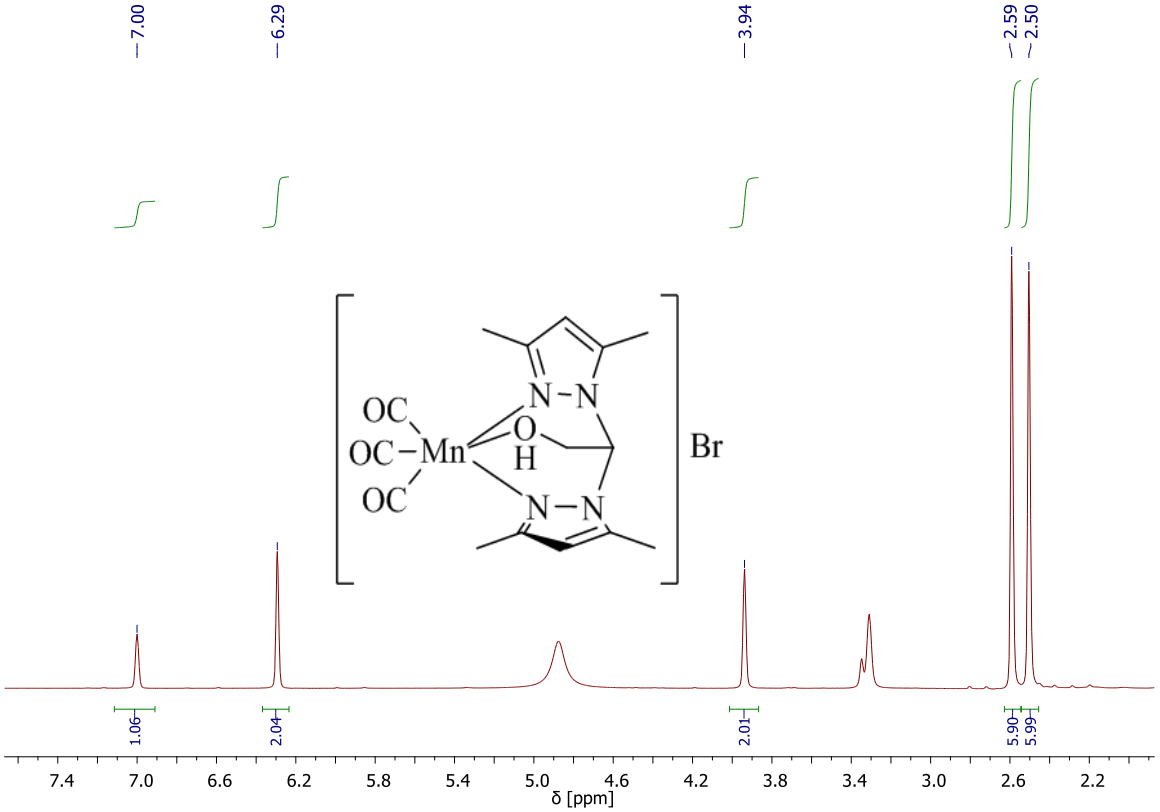

Figure S7: ^{1}H-NMR spectrum of [{Bis(3,5-dimethylpyrazol-1-yl)ethanol}Mn(CO)$_3$]Br in CD_3OD.

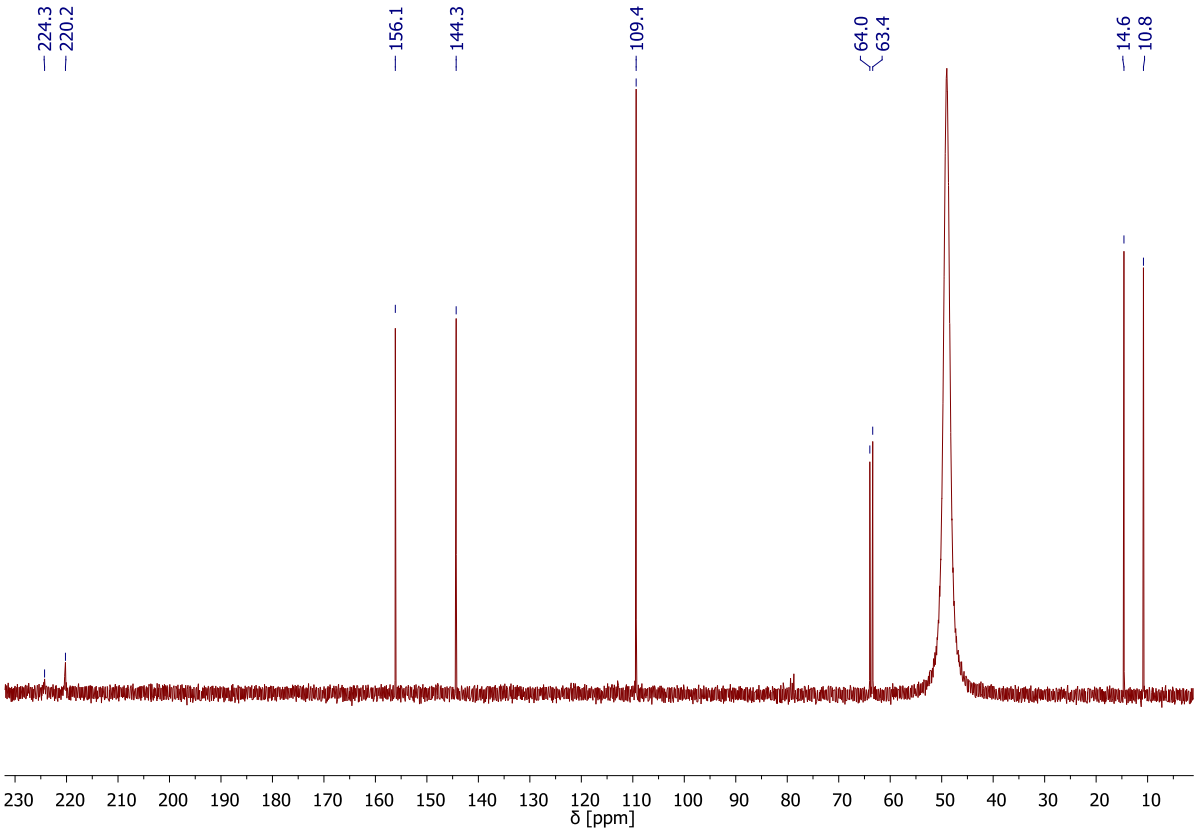

Figure S8: $^{13}C\{^{1}H\}$-NMR spectrum of [{Bis(3,5-dimethylpyrazol-1-yl)ethanol}Mn(CO)$_3$]Br in CD_3OD.

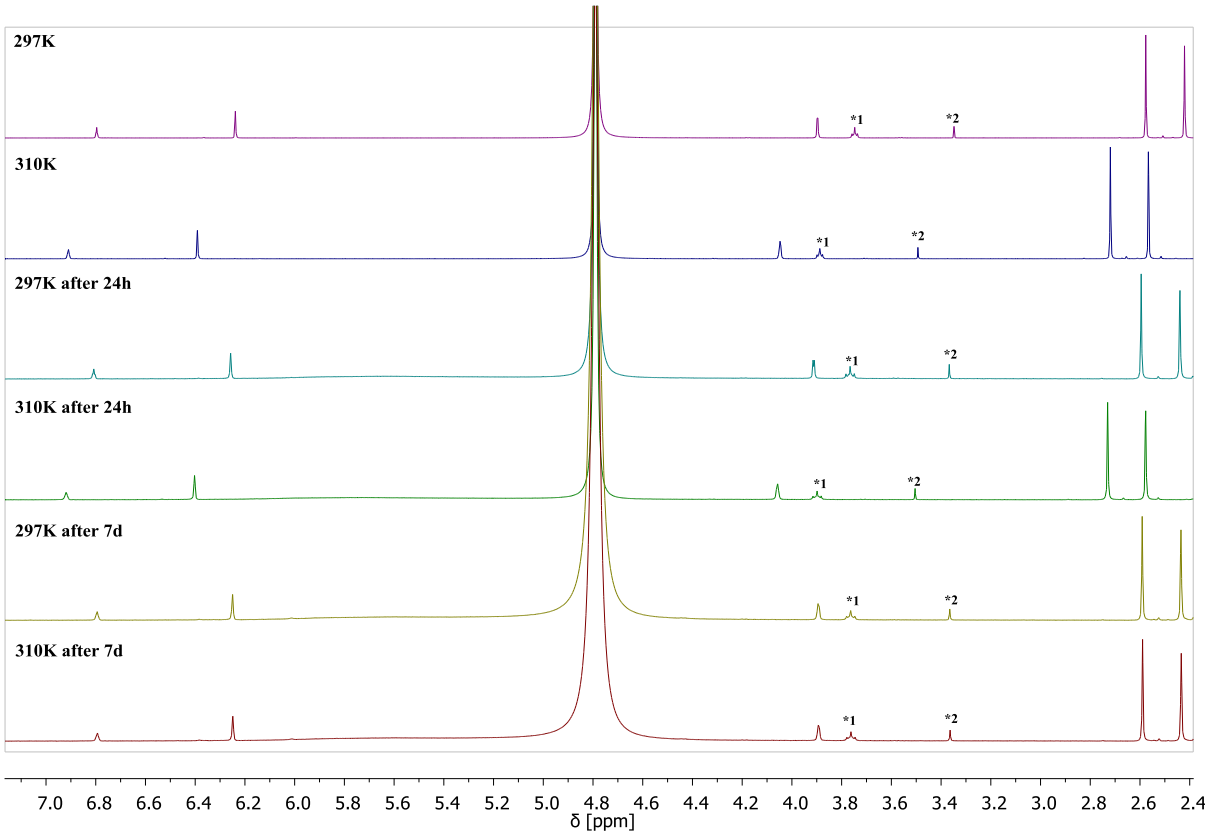

Figure S9: ^{1}H-NMR of CORM-ONN1 (**3**) in D_2O after 0h, 24h, and 7d at 297K and 310K; *1 = THF, *2 = MeOH.

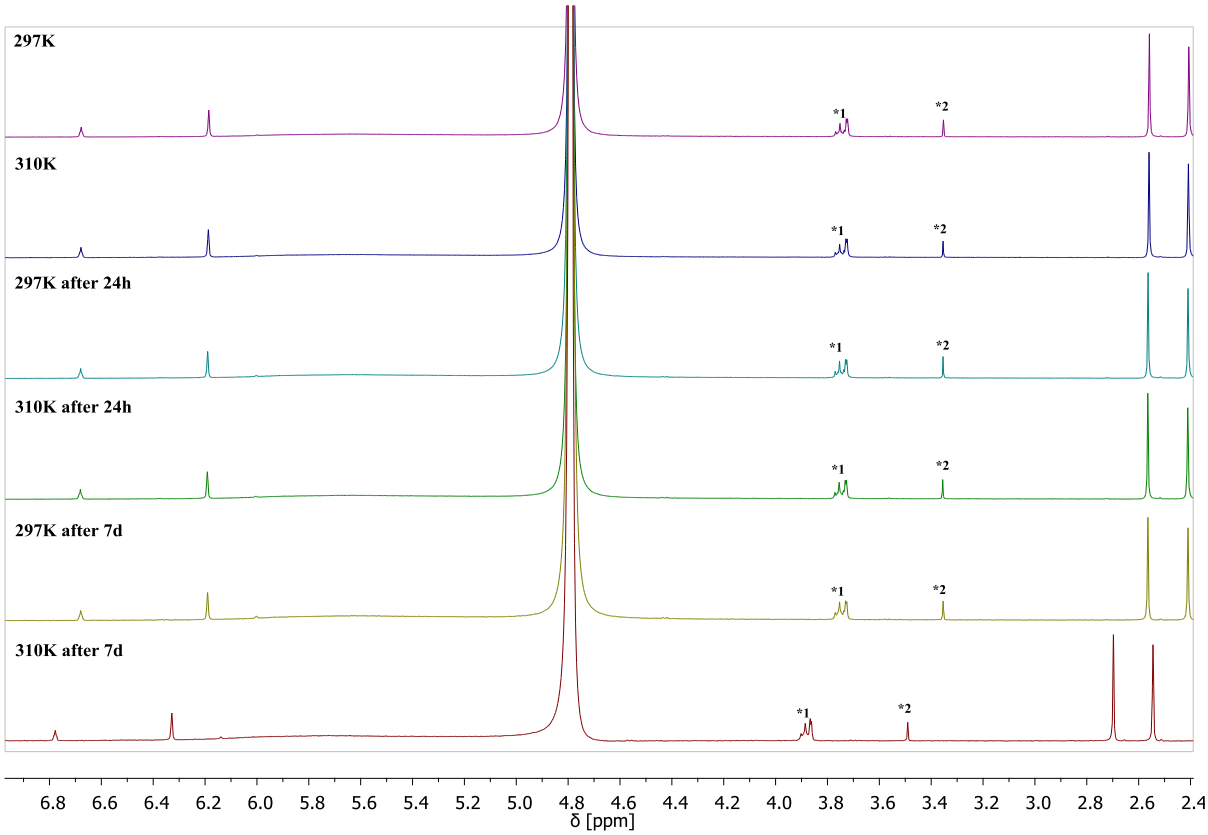

Figure S10: ^{1}H-NMR of CORM-ONN1 (**3**) in D_2O containing PBS after 0h, 24h, and 7d at 297K and 310K; *1 = THF, *2 = MeOH.

Degradation Product of [{Bis(3,5-dimethylpyrazol-1-yl)ethanol}Mn(CO)$_3$]Br (4) in MeOH

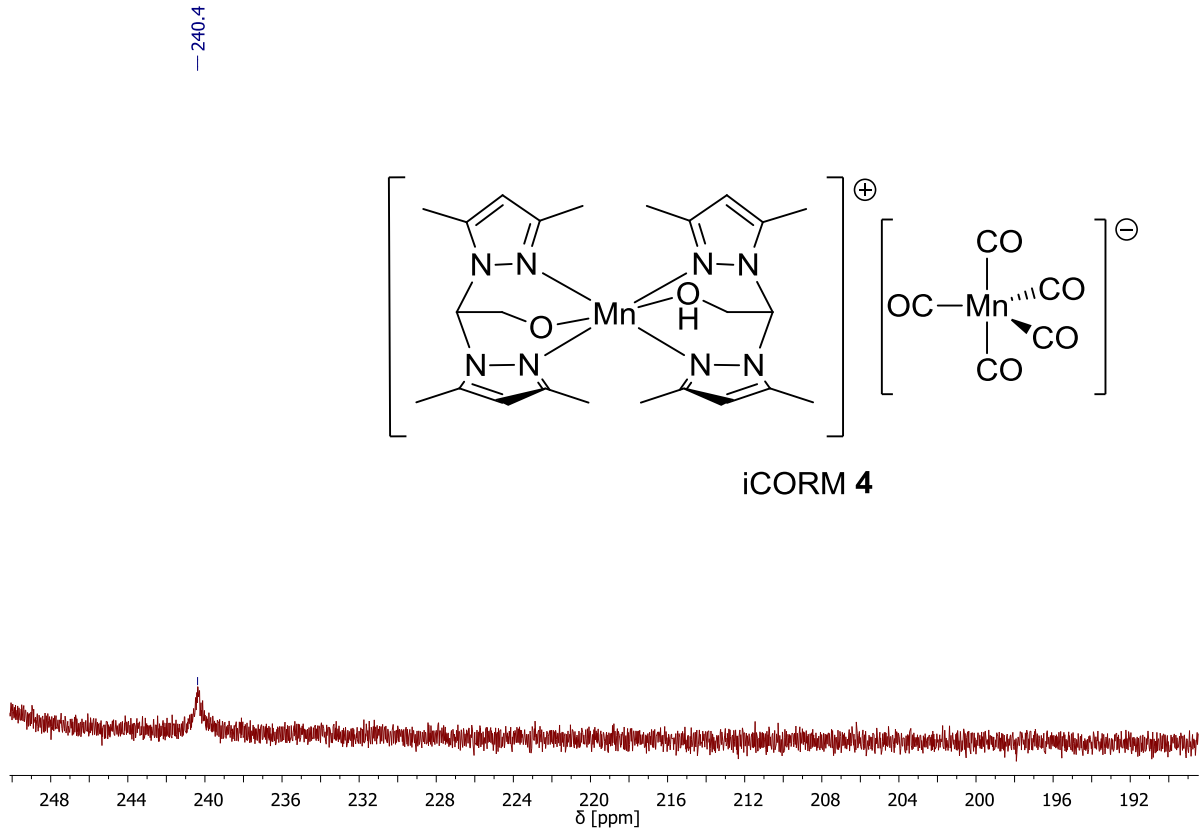

Figure S11: $^{13}C\{^{1}H\}$-NMR spectrum of the degradation product **4** in [D_8]THF.

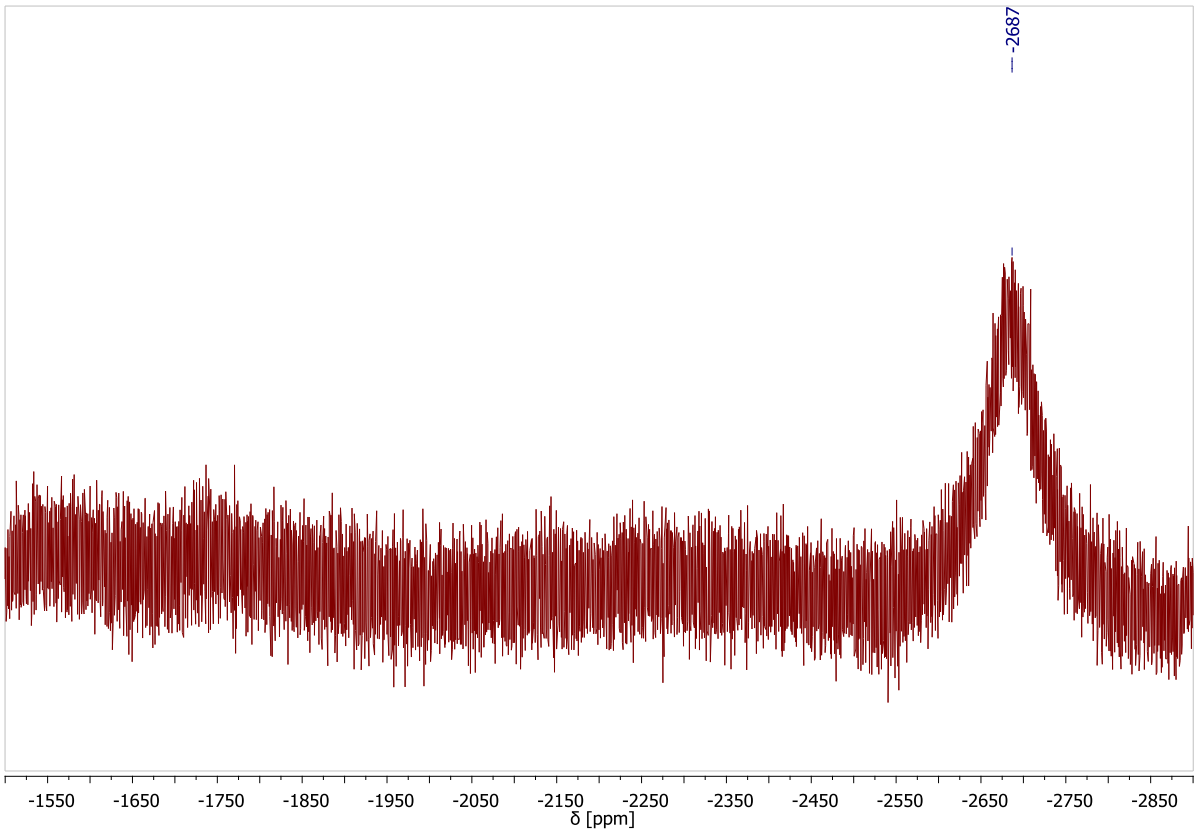

Figure S12: ^{55}Mn-NMR spectrum of the degradation product **4** in [D_8]THF.

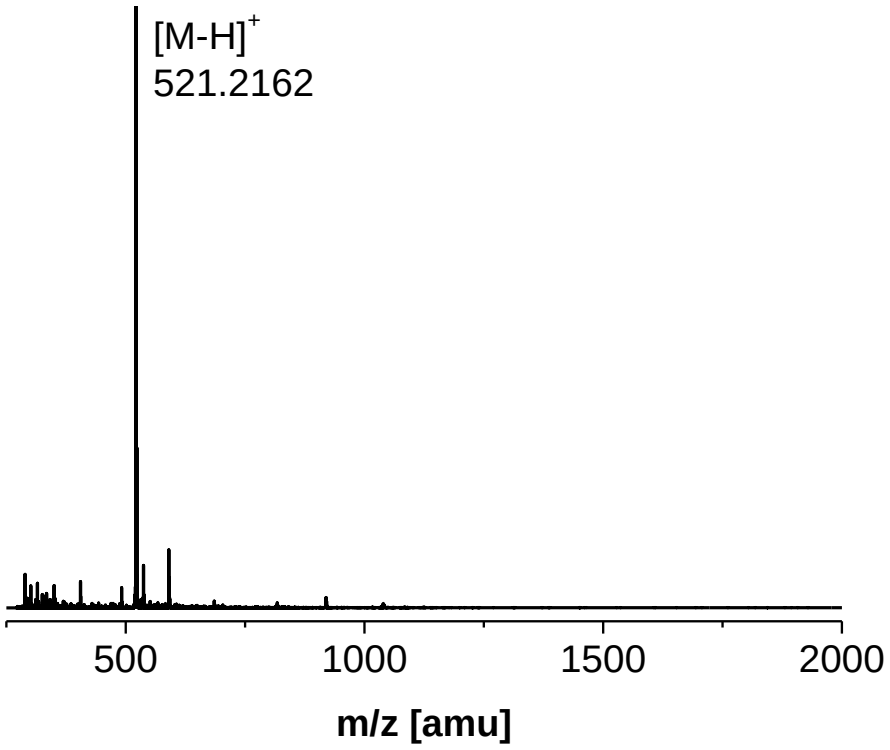

Figure S13: ESI-ToF-MS spectrum of **4**.

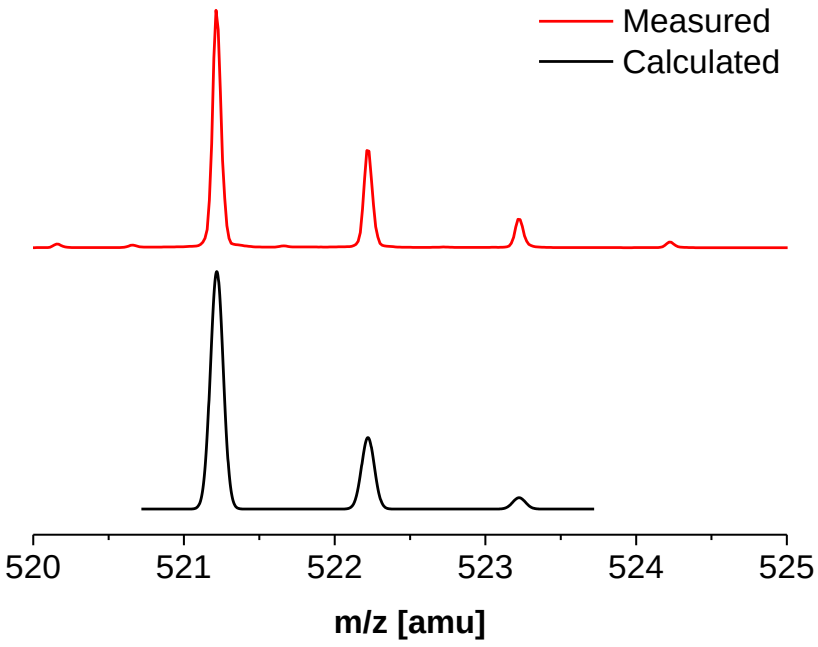

Figure S14: Comparison of measured and calculated isotope pattern of the peak of $[C_{24}H_{34}MnN_8O_2]^+$ of complex **4**.

CO Release Properties

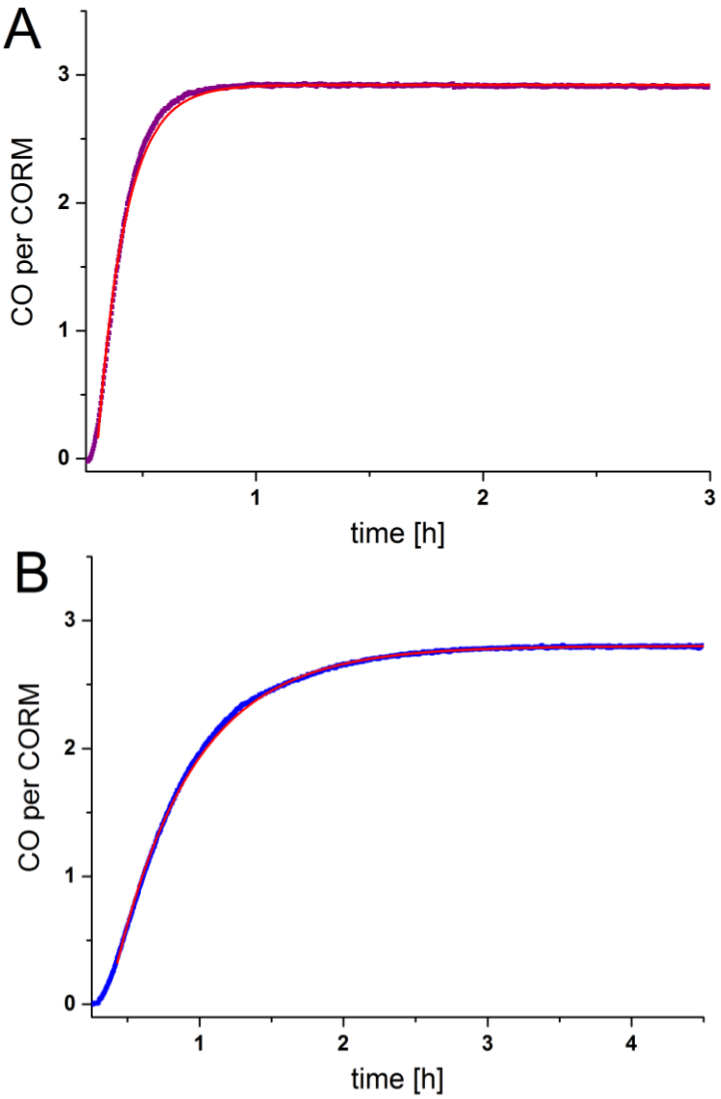

Figure S15: Amount of CO released in the gas phase per CORM as a function of the reaction time. The CO amount was measured above solutions of CORM-CONN1. The irradiation with light at 405 nm (**A**) and 470 nm (**B**) was switched on after 15 min. The mono-exponential function $y_0 + A(1 - e^{-(t-t_0)/\tau})$ representing a first order reaction kinetic was fitted to the data of each measurement. The starting time t_0, the asymptotic value A and the time constant τ were used as free parameters, while the offset y_0 was set to the value determined before the beginning of the irradiation. The starting time t_0 is the sum of the time starting the irradiation and a delay caused by diffusion (see: M. Klein, U. Neugebauer, A. Gheisari, A. Malassa, T. Jazzazi, F. Froehlich, M. Westerhausen, M. Schmitt, J. Popp, *J. Phys. Chem. A* **2014**, *118*, 5381-5390). The calculated time constants for CORM-ONN1 are means ± confidence intervals of 95%. For a better overview only the average values for each irradiation wavelength are shown. It is assumed that the irradiation intensity is constant during the entire reaction. A decrease of the irradiation intensity of less than 7% due to absorption by the CORM is assumed to not affect the profile of the first order reaction kinetic.

Myoglobin Assays

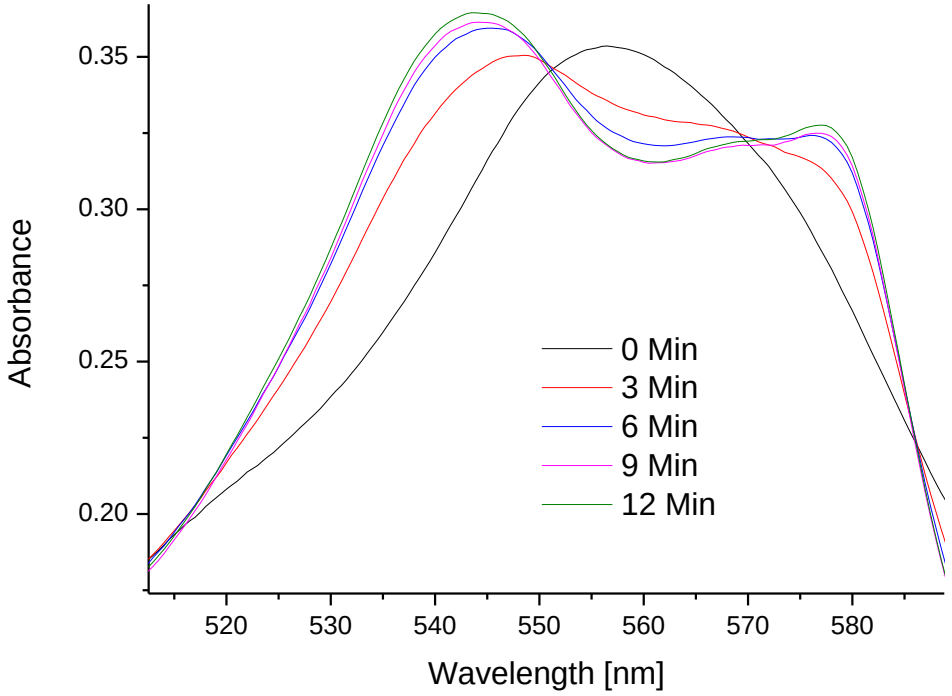

Figure S16: Myoglobin assay of CORM-ONN1 (irradiation with 365 nm, P = 1.58 mW).

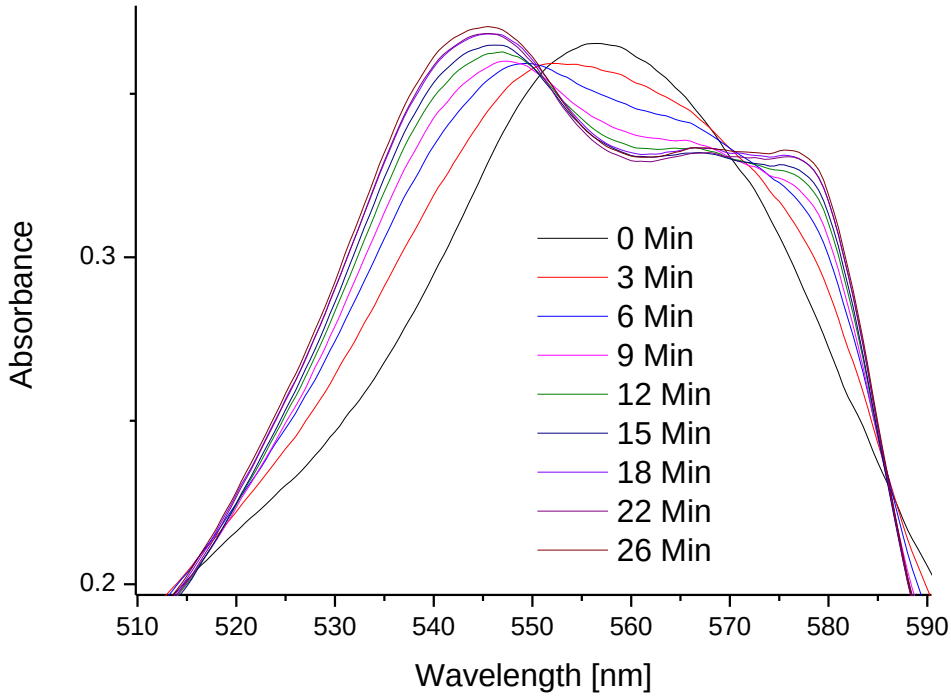

Figure S17: Myoglobin assay of CORM-ONN1 (irradiation with 405 nm, P = 2.48 mW).

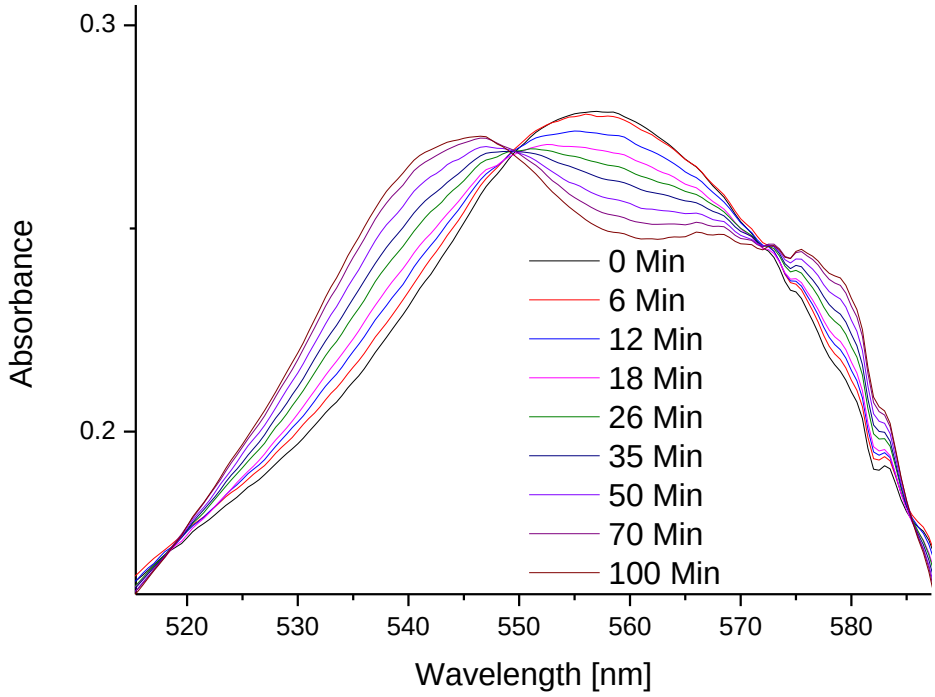

Figure S18: Myoglobin assay of CORM-ONN1 (irradiation with 480 nm, P = 2.50 mW).

Table S1: Max. CO per CORM by irradiation with different wavelengths.

Irradiation with	**Max. CO per CORM-ONN1**
365 nm	1.78
405 nm	1.90
480 nm	1.37

UV-Vis Spectrum and Quantum Yield

Calculation of the quantum yield Φ

$$\Phi(\lambda) = \frac{numbers\ of\ events}{number\ of\ photons\ absorbed}$$

$$= \frac{amount\ of\ reactant\ consumed}{amount\ of\ photons\ absorbed} = \frac{\frac{dx}{dt}}{q_0\left[1 - 10^{-Abs(\lambda)}\right]}$$

where $\frac{dx}{dt}$ is the rate of change of a measurable quantity, q_0 the amount of photons incident per time interval and Abs the absorbance (Source: S. E. Braslavsky, *Pure Appl. Chem.* **2007**, *79*(3), 293-465, Glossary of terms used in photochemistry, 3rd edition (IUPAC Recommendations 2006), pages 406-407).

The UV-VIS spectrum of CORM-ONN1 before and after irradiation in Figure S19 shows that the absoprtion band with its maximum at 360 nm vanished completly. Thus, also the absorptions of CORM-ONN1 at 405 nm and 470 nm were disappearing during the decay reaction of CORM-ONN1. The intensity difference caused by this decreasing absorption of CORM-ONN1 is neglegted for the estimation of the quantum yield. This intensity difference can be up to 13 % (between start and end of reaction) for an irradiation at 405 nm and 0.3 % at 470 nm. Therefore, photons incident per time interval q_0 is assumed to be constant.

When the Beer-Lambert law is applied to describe the absorbance Abs, the following function for the quantum yield is received depending on the concentration c.

➔ (2.) $$\Phi(\lambda) = \frac{V \cdot N_A \cdot \frac{dc}{dt}}{q_0\left[1 - 10^{-c(t)\cdot\epsilon\cdot l}\right]}$$

where $c(t)$ [mol/l] is the CORM concentration in solution at the time t, while l [cm] is the path length of the irradiated sample, $\epsilon(\lambda)$ [l·mol^{-1}·cm^{-1}] the extinction coefficient and q_0 [s^{-1}] the number of photons incident per time interval. $\frac{dc}{dt}$ is the derivation of the concentration at the time point t and the volume of the solution $V = A \cdot l$ is given by the base area A and the path length l.

The number of photons incident per time interval q_0 [s^{-1}] is calculated by using the irradiation power per area I_0 [mW/cm²], the wavelength λ [nm], the base area A [cm²], the Planck constant h [J·s], the speed of light c_{light} [m/s].

with $$q_0 = \frac{I_0 \cdot A}{E_{photon}} = \frac{I_0 \cdot A \cdot \lambda}{h \cdot c_{light}} \cdot 10^{-12}$$ ➔ $$\frac{q_0}{A} = \frac{I_0 \cdot \lambda}{h \cdot c_{light}} \cdot 10^{-12}$$

Since all measured absorbance values are smaller than 0.15, we use an appoximation for the calculation of the quantum yield $\Phi(\lambda)$:

$$10^{-Abs(\lambda)} = e^{-\ln(10)\cdot Abs(\lambda)} \approx 1 - \ln(10) \cdot Abs(\lambda) \quad \text{for} \quad Abs(\lambda) < 0.1 \quad 5$$

➔ $$\Phi(\lambda) \approx \frac{V \cdot N_A \cdot \frac{dc}{dt}}{q_0\left[1 - \left(1 - \ln(10) \cdot Abs(\lambda)\right)\right]} = \frac{V \cdot N_A \cdot \frac{dc}{dt}}{q_0 \cdot \ln(10) \cdot c(t) \cdot \epsilon \cdot l}$$

We conclude form Figure S15 that the CORM decay reaction can be describe by a first order reaction resulting in the following concentration profile for the starting material:

$$c_{CORM}(t) = c_0 \cdot e^{-\frac{t-t_0}{\tau}} \quad \rightarrow \quad \frac{dc}{dt}c = -\frac{1}{\tau} \cdot c$$

$$\rightarrow \quad \Phi(\lambda) \approx \frac{A \cdot l \cdot N_A \cdot \frac{1}{\tau} \cdot c(t)}{q_0 \cdot \ln(10) \cdot c(t) \cdot \epsilon \cdot l} = \frac{N_A}{\frac{q_0}{A} \cdot \ln(10) \cdot \epsilon \cdot \tau}$$

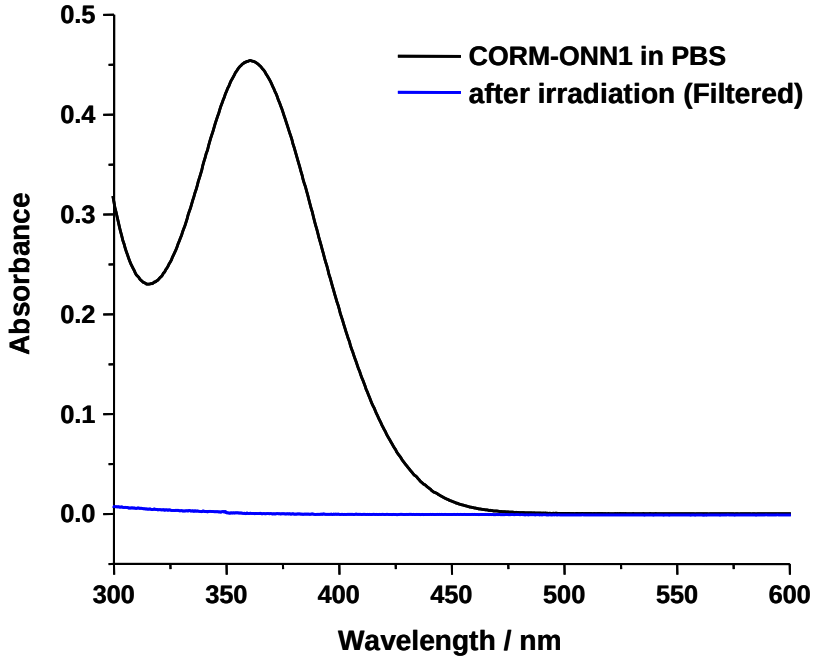

Figure S19: UV-VIS absorption spectrum of CORM-ONN1 in PBS (250 µM) before and after irradiation.

Molecule Representations:

Figure S20: Molecular structure and numbering scheme of [{(Pz^{Me2})$_2$$CH_2$}Mn(CO)$_3$Br] (**1B**, monoclinic modification). The ellipsoids represent a probability of 30 %. Hydrogen atoms are neglected for clarity reasons. Selected bond lengths (pm): Mn1-Br1 257.46(4), Mn1-N2 211.7(2), Mn1-N4 209.8(2), Mn1-C12 180.6(2), Mn1-C13 180.0(2), Mn1-C14 181.1(2), C12-O1 115.1(3), C13-O2 112.1(3), C14-O3 114.8(3); angles (deg.): Br1-Mn1-N2 96.01(5), Br1-Mn1-N4 92.48(5), Br1-Mn1-C12 84.57(7), Br1-Mn1-C13 173.20(8), Br1-Mn1-C14 83.65(7), N2-Mn1-N4 85.38(7), N2-Mn1-C12 96.49(9), N2-Mn1-C13 88.46(9), N2-Mn1-C14 178.60(9), N4-Mn1-C12 176.65(9), N4-Mn1-C13 92.99(9), N4-Mn1-C14 93.28(9), C12-Mn1-C13 89.84(10), C12-Mn1-C14 84.83(10), C13-Mn1-C14 92.00(10).

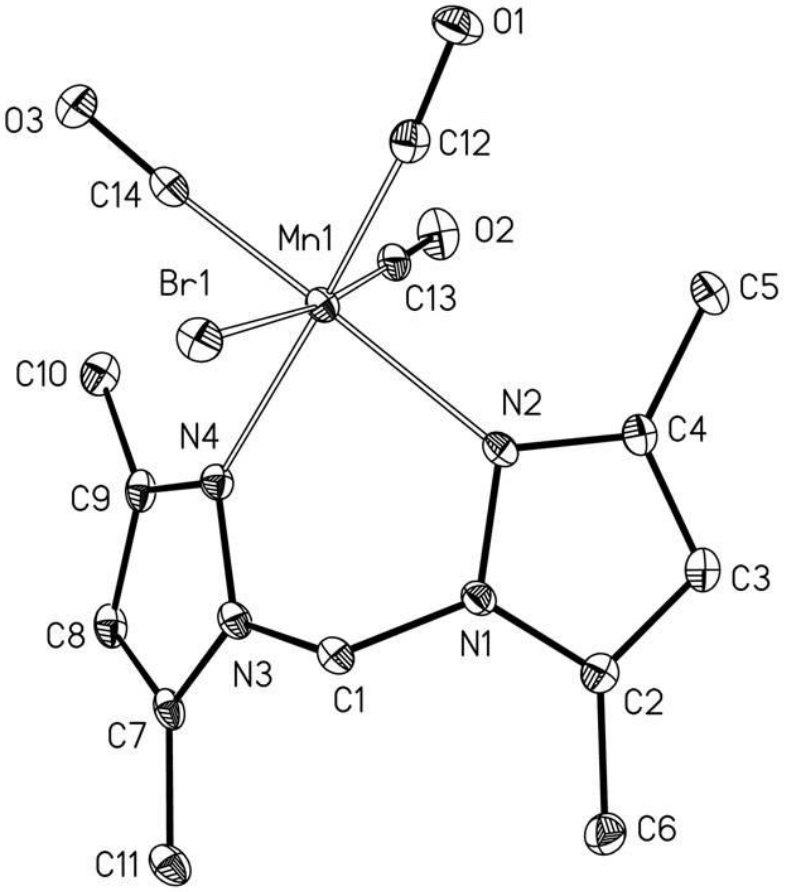

Figure S21: Structure and numbering scheme of the anion $[Mn(CO)_5]^-$ of iCORM **4**. The asymmetric unit contains two molecules A and B, only the anion of A is depicted. The ellipsoids represent a probability of 30 %. Selected bond lengths (pm) of anion A: Mn2-C25 179.3(3), Mn2-C26 179.8(3), Mn2-C27 181.2(3), Mn2-C28 181.8(3), Mn2-C29 182.1(4), C25-O3 116.4(4), C26-O4 116.0(4), C27-O5 115.2(4), C28-O6 115.8(4), C29-O7 115.4(4); angles (deg.): C25-Mn-C26 115.8(2), C25-Mn2-C27 125.4(1), C26-Mn-C27 118.8(1), C25-Mn-C28 91.0(2), C25-Mn-C29 88.7(2), C26-Mn-C28 92.4(1), C26-Mn-C29 92.5(1), C27-Mn-C28 88.0(2), C27-Mn-C29 87.9(2), C28-Mn-C29 174.8(1).

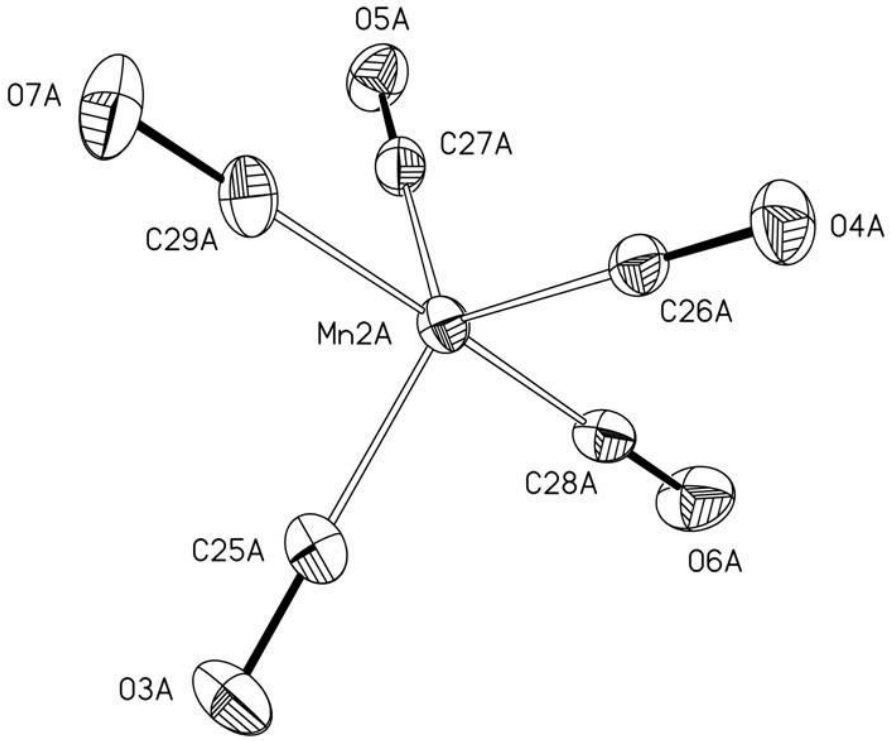

Figure S22: Ball-and-stick representation of the structure of iCORM **4**, the degradation product of CORM-ONN1. The atoms are drawn with arbitrary radii, carbon-bound hydrogen atoms are neglected for clarity reasons. In the middle the dinuclear cation is shown, hydrogen bridges are clarified by broken lines. The $[Mn(CO)_5]^-$ anions are located besides the complex cation without short distances between anion and cation.

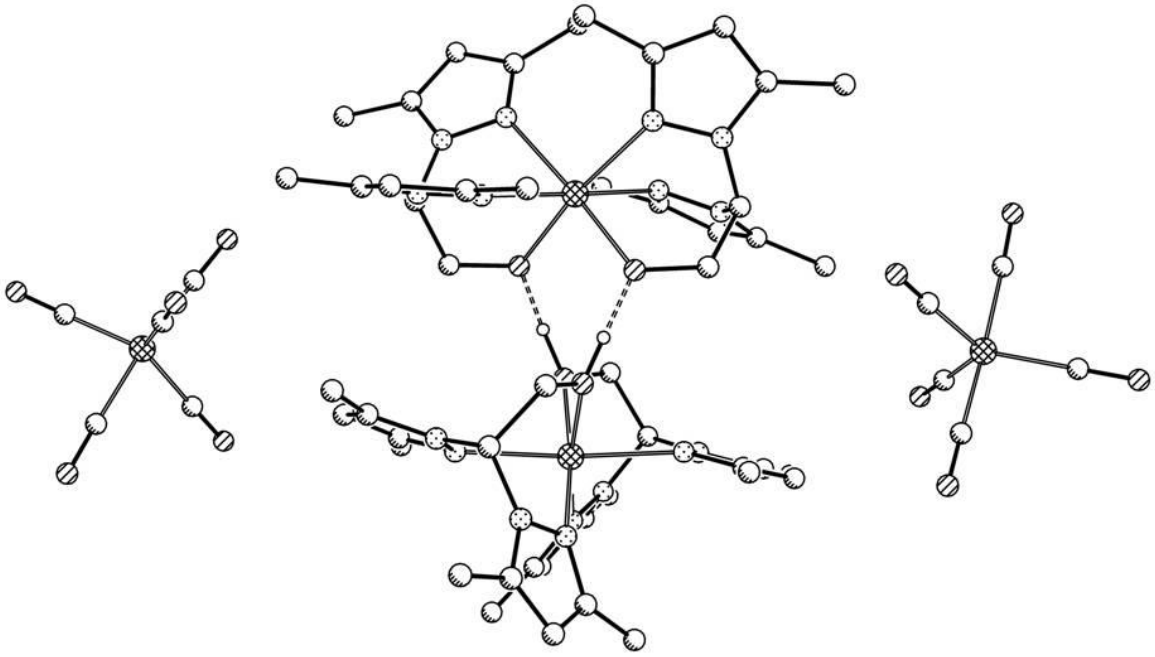

Figure S23: Molecular structure and numbering scheme of $(Pz^{Me2})_2CH\text{-}CH_2\text{-}OH$ (top) and aggregation via hydrogen bridges (bottom). The ellipsoids represent a probability of 30 %. Hydrogen atoms are shown with arbitrary radii. Selected bond lengths (pm):O1-C2 141.2(2), O1-$H1_{O1}$ 90(3), N1-C3 135.9(2), N1-N2 136.9(2), N1-C1 145.4(2), N2-C5 133.3(2), N3-C8 135.9(2), N3-N4 136.6(2), N3-C1 146.2(2), N4-C10 133.1(2), C1-C2 153.0(2), C3-C4 137.2(2), C3-C7 149.3(2), C4-C5 140.7(2), C5-C6 149.2(2), C8-C9 137.4(2), C8-C12 148.9(2), C9-C10 140.3(2), C10-C11 149.5(2).

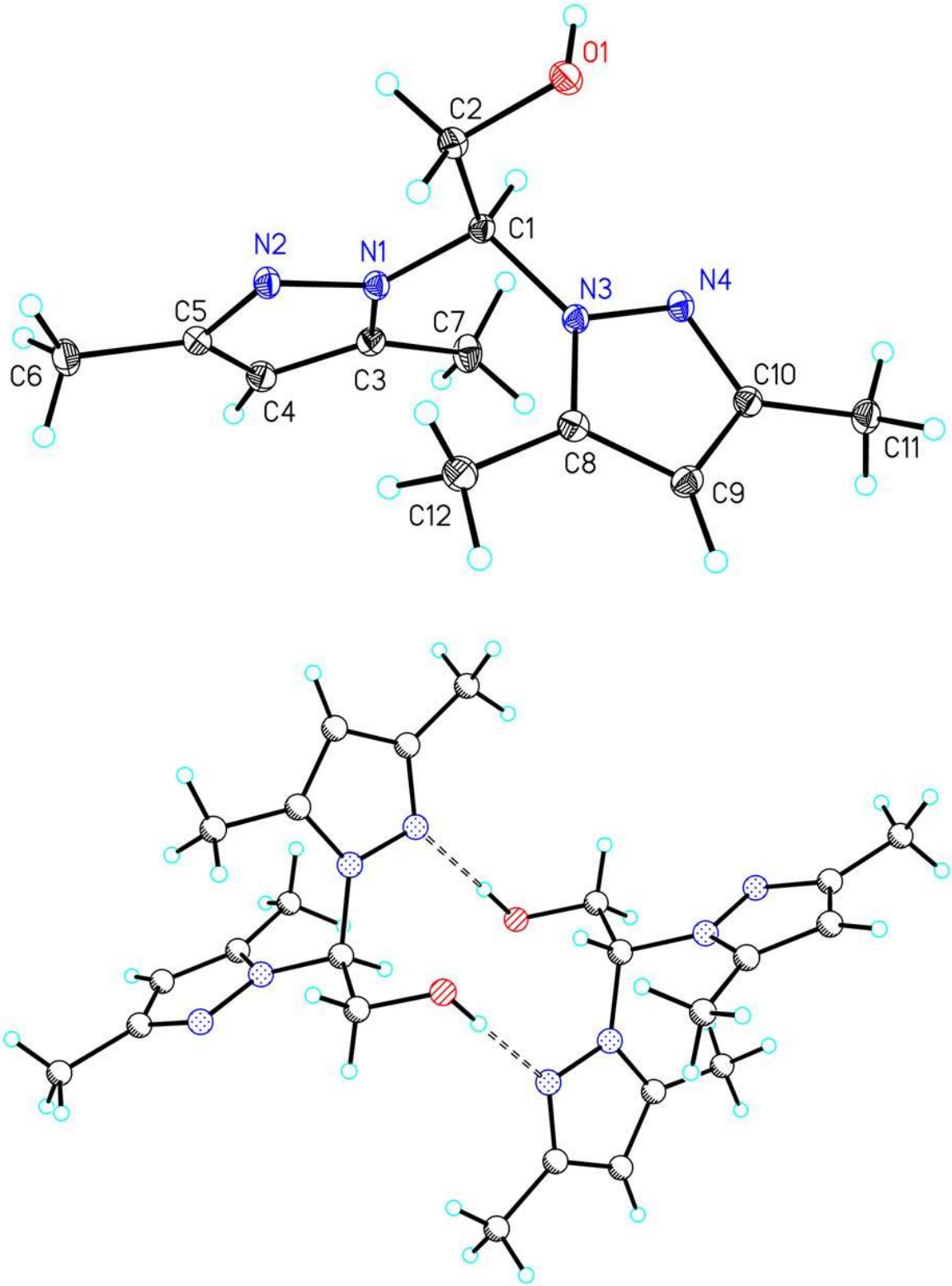

Table S2: Crystal data and refinement details for the X-ray structure determinations of the compounds **1** - **2**.

Compound	**1A**	**1B**	**2**
formula	$C_{14}H_{16}BrMnN_4O_3$	$C_{14}H_{16}BrMnN_4O_3$	$C_{15}H_{15}MnN_4O_5$
fw ($g \cdot mol^{-1}$)	423.16	423.16	386.25
°*C*	-140(2)	-140(2)	-140(2)
crystal system	orthorhombic	monoclinic	triclinic
space group	P n m a	P 2_1/n	P ī
a/ Å	10.0995(2)	9.3065(3)	8.1397(2)
b/ Å	14.5864(3)	10.6722(3)	10.3669(3)
c/ Å	11.3819(2)	16.7643(5)	10.7821(2)
α/°	90	90	103.904(2)
β/°	90	98.598(1)	111.361(1)
γ/°	90	90	91.846(1)
V/Å^3	1676.73(6)	1646.33(9)	815.25(3)
Z	4	4	2
ρ ($g \cdot cm^{-3}$)	1.676	1.707	1.573
μ (cm^{-1})	31.89	32.48	8.45
measured data	3607	11926	6395
data with I > 2σ(I)	1874	3412	3519
unique data (R_{int})	1980/0.0144	3724/0.0343	3667/0.0133
wR_2 (all data, on F^2)[a)]	0.0461	0.0660	0.0606
R_1 ($I > 2\sigma(I)$) [a)]	0.0214	0.0281	0.0256
S [b)]	1.101	1.116	1.046
Res. dens./$e \cdot Å^{-3}$	0.329/-0.253	0.586/-0.509	0.356/-0.337
absorpt method	multi-scan	multi-scan	multi-scan
absorpt corr $T_{min}/_{max}$	0.6543/0.7456	0.6231/0.7456	0.6996/0.7456
CCDC No.	1488835	1488836	1488837

Table S2 (contd.): Crystal data and refinement details for the X-ray structure determinations of the compounds **3 - $(Pz^{Me2})_2CH\text{-}CH_2OH$**.

Compound	**3**	**4**	**$(Pz^{Me2})_2CH\text{-}CH_2OH$**
formula	$C_{15}H_{18}BrMnN_4O_4$	$C_{29}H_{35}Mn_2N_8O_7$	$C_{12}H_{18}N_4O$
fw ($g\cdot mol^{-1}$)	453.18	717.53	234.30
°*C*	-140(2)	-140(2)	-140(2)
crystal system	monoclinic	triclinic	triclinic
space group	P 2_1/c	P $\bar{1}$	P $\bar{1}$
a/ Å	13.8488(2)	11.6573(3)	7.4242(2)
b/ Å	11.0641(3)	14.7441(3)	8.6729(3)
c/ Å	11.6952(2)	20.6894(5)	10.7671(4)
α/°	90	85.371(2)	99.558(2)
β/°	98.380(1)	81.709(1)	103.319(2)
γ/°	90	69.787(1)	111.723(2)
V/Å^3	1772.86(6)	3300.32(13)	602.02(3)
Z	4	4	2
ρ ($g\cdot cm^{-3}$)	1.698	1.444	1.293
μ (cm^{-1})	30.26	8.22	.86
measured data	12429	38249	3831
data with I > 2σ(I)	3679	11312	2392
unique data (R_{int})	4031/0.0270	14363/0.0360	2718/0.0217
wR_2 (all data, on F^2)[a)]	0.0565	0.1316	0.1187
R_1 ($I > 2\sigma(I)$) [a)]	0.0248	0.0488	0.0514
S [b)]	1.063	1.057	1.070
Res. dens./$e\cdot Å^{-3}$	0.365/-0.354	0.795/-1.004	0.282/-0.261
absorpt method	multi-scan	multi-scan	multi-scan
absorpt corr $T_{min}/_{max}$	0.6705/0.7456	0.6329/0.7456	0.6782/0.7456
CCDC No.	1488838	1488839	1505640

[a)] Definition of the *R* indices: $R_1 = (\Sigma \,||F_o| - |F_c||)/\Sigma |F_o|$;
$wR_2 = \{\Sigma[w(F_o^2-F_c^2)^2]/\Sigma[w(F_o^2)^2]\}^{1/2}$ with $w^{-1} = \sigma^2(F_o^2) + (aP)^2$+bP; $P = [2F_c^2 + Max(F_o^2]/3$;
[b)] $s = \{\Sigma[w(F_o^2-F_c^2)^2]/(N_o-N_p)\}^{1/2}$.